Chemical Physics Letters 842 (2024) 141225

Contents lists available at ScienceDirect

Chemical Physics Letters

journal homepage: www.elsevier.com/locate/cplett

Research paper

High activity and CH_4 selectivity for photocatalytic CO_2 reduction by Cu modified C_3N_4 nanotubes

Ye Liu [1], Lei Zhang [1], Yubo Kuang, Xiaoqian Xiang, Haohan Tao, Guangran Di, Xiaojing Yin, Meicheng Li, Xiao-Jun Lv [*]

State Key Laboratory of Alternate Electrical Power System with Renewable Energy Sources, School of New Energy, North China Electric Power University, Beijing 102206, PR China

ARTICLE INFO

Keywords:
Photocatalysis
CO_2 reduction
Cu modified C_3N_4
Tubular
High selectivity

ABSTRACT

The photocatalytic CO_2 reduction has the problems of low selectivity of single product. Here, the preparation of Cu modified tubular C_3N_4 (CTN) was studied. The increase of the active site inhibits the recombination of electrons (e-) and holes (h +) and improves the selectivity of CO_2 reduction products. Finally, the CO and CH_4 yields of 1.5 % CTN photocatalyst are 11.55 μmol·g^{-1} and 4.72 μmol·g^{-1}, respectively, which are 5 times higher than that of tubular C_3N_4 photocatalyst. The selectivity of 2 % CTN to CH_4 is up to 68 %, indicating that the prepared CTN photocatalyst has high CO_2 reduction activity and CH_4 selectivity.

1. Introduction

With the increasing population, the total energy requirement for human social activities has continued to rise. CO_2 emission reduction and sustainable development has become the focus of common attention of all countries in the world. According to the forecast of the International Climate Change Special Committee (IPCC), in 2100, the CO_2 content in the air may increase to 590 ppm, and the global average temperature may increase by 1.9 °C [1]. The photocatalytic technology can use green and pollution-free solar resources to complete a variety of catalytic reactions with the help of catalysts, such as water decomposes to produce hydrogen, CO_2 reduction, degradable organic pollutants, etc. Having high efficiency and economical catalysts is of very important for the development of photocatalysis.

Graphite carbon nitride (g-C_3N_4) is a kind of non-metallic photocatalyst. Due to its low cost, simple preparation process and good light absorption performance, it has received extensive attention. For instance, Antonietti group found that the porous g-C_3N_4 rich in surface groups could be applied to Friedel-Crafts reaction, which opened the development of g-C_3N_4 in the catalytic field [2]. g-C_3N_4 is a material with a suitable bandgap (2.7–2.8 eV) and has been fully applied in the direction of photocatalysis. As a result of extensive sources, nontoxic, stability, and relatively narrow bandgap, and has the characteristics of visible light response, g-C_3N_4 is considered a catalyst with prospects. But there are some problems. First of all, the shape of the material is irregular, and the material is thick, which affects the process of separation and oxidation reaction of its carriers. Then due to carrier has high recombination velocity, it is prone to the problem of compounding as soon as it is stimulated, resulting in low optical catalytic performance. The conduction band (CB) potentials of g-C_3N_4 material is relatively positive, so optical electronics has lower energy. This will cause the reaction rate slowly when the reaction is performed. In addition, the material is irregular on the surface of the block structure and lacks adsorption nodes, which limits the utilization efficiency of carriers and affects its performance in photocatalytic. In order to solve these problems, methods such as appearance regulation [3–8], element doping [9–11], and heterogeneous knots [12,13] are used to improve the catalytic activity of g-C_3N_4.

For CO_2 reduction, in addition to the appearance structure, it is necessary to further improve the optical catalytic efficiency by adjusting the electronic structure and building more charge transfer channels. In the strategy of adjusting the electronic structure of the optical catalyst, doping is the most commonly used method. By doping atoms, the band gap is improved, affecting the CB potentials and valence band (VB) potentials. In addition, in the field of CO_2 reduction, the metallic Cu base optical catalyst has also received widespread attention. Pei et al. synthesized and reported the ZnO-Cu(I) hybrid nanoparticles, which can directly convert CO_2 to CH_4 in the H_2O with normal temperature and

* Corresponding author.
E-mail address: lvxiaojun@ncepu.edu.cn (X.-J. Lv).
[1] Ye Liu and Lei Zhang have the equal contribution.

https://doi.org/10.1016/j.cplett.2024.141225
Received 22 January 2024; Received in revised form 20 March 2024; Accepted 20 March 2024
Available online 21 March 2024

pressure. The experiment shows that the maximum yield of CH_4 is 1080 $\mu mol \cdot g^{-1} \cdot h^{-1}$, the quantum production rate is 1.5 %, and the selectivity of CH_4 is almost 100 % [14]. Juliana 's team deposited Cu^0 nanoparticles on the surface of TiO_2. With the formation of heterostructures, the activity of the photocatalyst increased, and in addition to C_1 products (CH_4, CO, and CH_3OH), products containing two or more carbons (C_{2+}) were also generated. Such as acetic acid ($C_2H_4O_2$), acetone (C_3H_6O) and isopropyl alcohol (C_3H_8O) [15]. The above studies show that Cu doping can improve the optical catalytic efficiency of the sample, increase the transfer of the photochemical carrier, increase the concentration of the reactive site on the catalytic surface, and improve the selectivity of the product during photocatalytic CO_2 reduction.

According to previous reports [16,17], tubular g-C_3N_4 (TCN) materials have been widely studied because of their mass transfer properties and high carrier transport efficiency. Cu loading on g-C_3N_4 is conducive to the formation of Cu-N_4 sites and promote the photocatalytic process [18]. Therefore, this work studies the photocatalytic CO_2 reduction performance based on TCN loaded with Cu on its surface under light irradiation. The morphology, properties and photocatalytic mechanism of the samples were characterized. In addition, the photocatalyst and the reaction system were optimized. The effects of the amount of Cu added and acetonitrile count on the photocatalytic CO_2 reduction performance of the catalyst were studied, and the optimal reaction conditions of the system were obtained.

2. Experimental section

2.1. Materials

Melamine ($C_3H_6N_6$, AR) and cupric chloride ($CuCl_2 \cdot 2H_2O$, AR) came from Shanghai Aladdin Biochemical Technology Co, Ltd. Acetonitrile (C_2H_3N, AR) were obtained from Beijing InnoChem Science & Technology Co., Ltd.

2.2. Synthesis of TCN and CTN

1 g of $C_3H_6N_6$ was added to a beaker and stirred at 80 °C for 0.5 h. Afterwards, the stirred solution was transferred into a 100 mL Teflon-lined high-pressure reactor. The reactor was then heated to 200 °C overnight. The resultant substance was subsequently washed and dried in a vacuum oven at 60 °C for 12 h until it became a white powder. 1 g of the previously obtained white powder was dissolved in 50 mL of H_2O, and a specific amount of $CuCl_2 \cdot 2H_2O$ was added. The sample underwent stirring at 80 °C for 1 h, then filtered and dried before being placed in a muffle furnace. The furnace was heated at a rate of 5 °C $\cdot min^{-1}$ in an argon atmosphere to a temperature of 550 °C for 2 h, resulting in the formation of Cu-loaded tubular C_3N_4 (CTN). $CuCl_2 \cdot 2H_2O$ was added in amounts of 0 mg, 15.3 mg, 30.6 mg, 45.9 mg, and 61.2 mg, corresponding to sample names of tubular g-C_3N_4 (TCN), 0.5 % CTN, 1 % CTN, 1.5 % CTN, and 2 % CTN respectively. The preparation process of the catalyst TCN and CTN were shown in Scheme 1.

2.3. Characterizations

Morphology of the catalysts were analysed by emission scanning electron microscope (SEM) (TM4000Plus, Hitachi Limited). Crystal structure of the catalysts were analysed by an X-ray diffractometer (XRD) (Smart Lab SE, Rigaku). Fourier transform infrared spectra (FT-IR) were studied using an FT-IR spectrometer (Bruker ALPHA, Bruker Optics). Compositions and chemical state of the catalysts were studied on an X-ray photoelectron spectroscopy (XPS). UV–Vis diffuse reflectance spectra (DRS) were employed with an UV–vis spectrophotometer (UV-2600i, Shimadzu Corporation) equipped with an integrating sphere diffuse reflectance accessory. The photoluminescence (PL) spectra of catalysts were studied on spectrofluorometer (LS 55, Perkin-Elmer). Mott-Schottky (MS) plots, photocurrent response and electrochemistry impedance spectroscopy (EIS) measurements were studied with a CHI electrochemical analyser (CHI760E) using a standard three-electrode mode with 0.2 M Na_2SO_4 solution as the electrolyte, Ag/AgCl (saturated KCl) as the reference electrode and a Pt sheet as the counter electrode.

2.4. Photocatalysis experiments

The photocatalytic CO_2 reduction experiment was conducted in a 65 mL sealed quartz reaction cell. Add acetonitrile and deionized water to the reactor, and then add 10 mg of sample. Stir and ultrasound for 10 min each. Introduce high-purity CO_2 (99.999 %) into the reactor for bubble degassing for another 0.5 h. 50 W LED were used for illumination and cool the reactor through air cooling. Analyze gas products using a gas chromatograph (GC-2014C). Collect gas products using a 1 mL syringe within a specified time interval and inject them into a gas chromatograph for analysis of their composition.

3. Results and discussion

3.1. Morphology and structure

The SEM tests exposed the morphology and structure of samples. As depicted in Fig. 1(a) and (b), CN demonstrated a hollow tube configuration. Fig. 1(a) reveals a smoother surface of TCN, with a pore diameter of approximately 1.07 μm. Conversely, the surface of 1.5 % CTN in Fig. 1 (b) appears more uneven, possibly due to Cu loading. The XRD pattern of the sample that was prepared is exhibited in Fig. 1(c). The distinctive diffraction peak at 27.5° in the figure is in correspondence with the (0 0 2) crystal plane [19] and all samples share the same diffraction peak. Because of the low Cu content in the product, the molecular structure of g-C_3N_4 remains virtually unaltered, therefore, there is no Cu peak in any

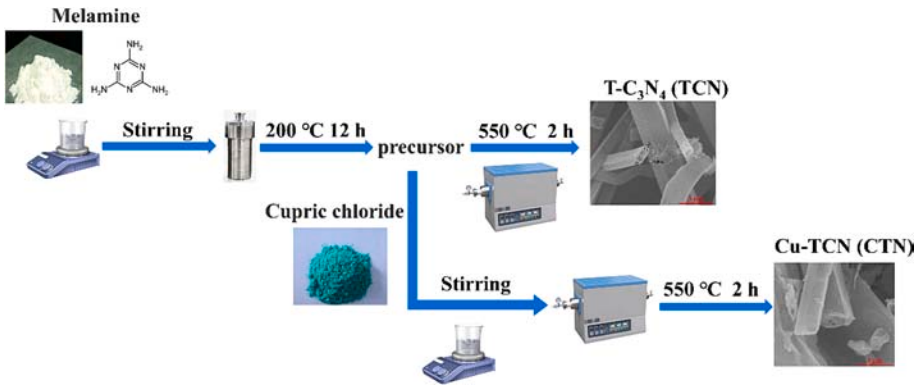

Scheme 1. Schematic diagram of preparation of TCN and CTN catalyst.

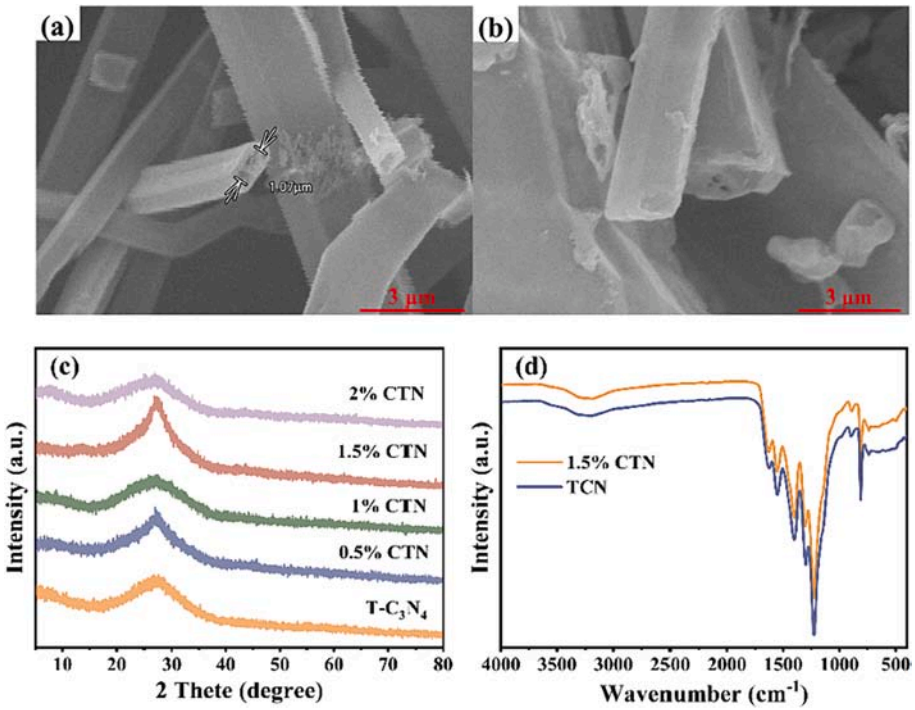

Fig. 1. (a) The SEM of TCN; (b) the SEM of 1.5% CTN; (c) XRD patterns and (d) FT-IR spectra of TCN and CTN.

of the CTN samples. Fig. 1(d) displays the FT-IR spectrum of the material. The FT-IR spectrum displays three prominent peaks: 1100 ~ 1650 cm^{-1}, 808 cm^{-1}, and 3170 cm^{-1}. The region of 1100 ~ 1650 cm^{-1} includes various strong bands that are typical of the expansion mode of CN heterocyclic rings. At 808 cm^{-1}, the spike in the signal is attributable to different vibration patterns of the C-N bond in the triazine ring, alongside the characteristic breathing patterns of the three-thin heterocyclic feature [20–22]. Furthermore, within the wide absorption band at approximately 3170 cm^{-1}, N-H and O-H bonds generate a range of vibration modes, which correspond to an uninterrupted amino group. 1.5 % CTN showed minor differences in peak position compared to TCN, with only a slight reduction in peak intensity [23]. The low Cu content makes it hard to detect, thus no vibration peaks of Cu-C or other Cu-N bonds are present in the spectrum. XRD and FT-IR spectroscopy results indicate that the catalyst were successfully synthesized.

The composition of CTN was determined via XPS analysis. Fig. 2(a) displays the full XPS spectrum which indicates that CTN is made up of C, N, O and Cu elements, confirming successful Cu integration. The appearance of the O1s peak could be attributed to sample adsorption in the atmosphere. Fig. 2(b) depicts the high-resolution XPS of C 1s, which

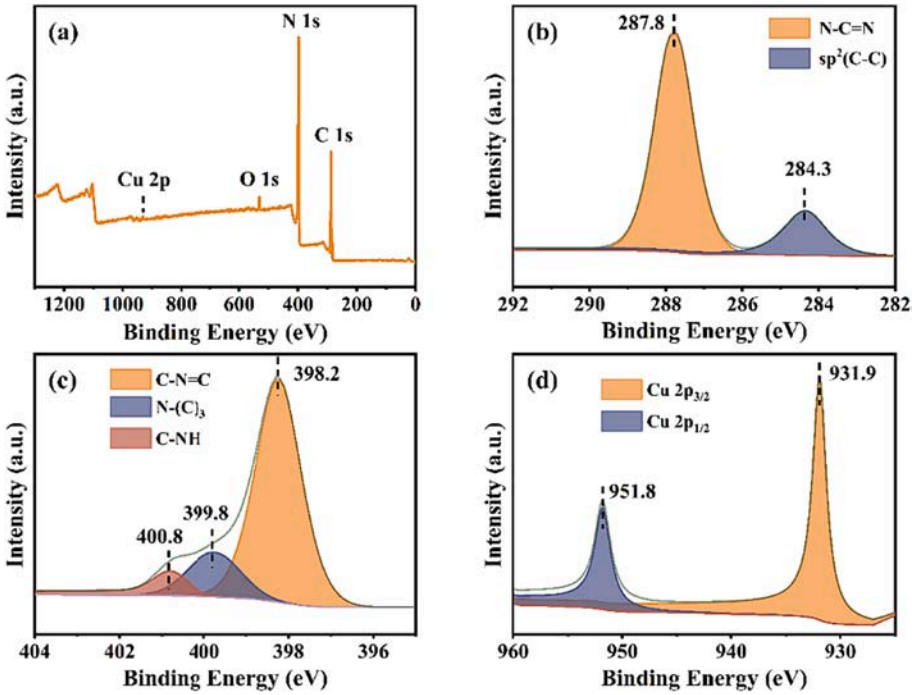

Fig. 2. XPS spectra of 1.5 % CTN: (a) survey spectrum; (b) C 1s; (c) N 1s and (d) Cu 2p spectra.

shows that CTN exhibits two peaks at 287.8 and 284.3 eV, corresponding to the hexazine ring (N-C = N) and sp^2 hybrid C in the SP^2 C-C bond, respectively [24,25]. Furthermore, the XPS analysis of N in CTN reveals three distinct peaks at 398.2 eV for C-N = C, 399.8 eV for N-(C)3, and 400.8 eV for C-N-H, as illustrated in Fig. 2(c) [26]. The high-resolution XPS of Cu 2p displayed in Fig. 2(d) displays two principal peaks at 951.8 eV and 931.9 eV, which can be assigned to the spin–orbit configurations of Cu^0 ($2p_{1/2}$ and $2p_{3/2}$), respectively [27].

The specific surface area and pore structure of the material were tested by N_2 adsorption–desorption method. As we all know, the larger the specific surface area, the more active sites can be exposed, the higher the activity of photocatalysis. It can be seen from Fig. 3(a) that the catalyst has a typical H3 hysteresis loop IV isotherm. Catalyst 1.5 % CTN has a wide pore size distribution (Fig. 3(b)). By comparing the data in Table 1, catalyst 1.5 % CTN has a larger specific surface area than pure TCN. These results indicate that Cu can be introduced into the catalyst to obtain larger specific surface area and pore volume. Therefore, it is inferred that the catalyst 1.5 % CTN has greater potential in photocatalytic CO_2 reduction.

3.2. Photocatalytic activity

First of all, we designed experiments to explore the photocatalytic activities of samples with different Cu loads. Fig. 4(a–b) and Fig. S1(a) show that the yield of CH_4 and CO had increased with the increase of Cu quality, and the maximum yield were 4.72 and 11.55 $\mu mol \cdot g^{-1}$, respectively. At the same time, the yield of H_2 had decreased, which significantly improved the selectivity of carbon products. The selectivity of CO and CH_4 were 36 % and 30 % of 1.5 % CTN sample. Noting, the CH_4 selectivity is best and can reach up to 68 % when we used the 2 % CTN photocatalysts as shown in Fig. 4b, which means that high Cu content can be beneficial to the CH_4 conversion. However, excess copper can obscure the active site and lead to decreased CH_4 selectivity (Fig. S1 (b)). The Selectivity (S) is calculated through the following formula:

$$S(\%) = \frac{nA}{\Sigma nA} \times 100\% \quad (1)$$

Where n is the number of reaction products transfer electrons and A is the yield of the reaction product. The introduction of Cu further improved the catalytic performance for the CO_2 reduction.

To evaluate the impact of solvents on the performance of catalysts, we set up a reaction system for four sets of acetonitrile and water (Fig. 4 (c–d)). With the increase of deionized water, the yield of H_2 had increased. It can be seen that in the reaction system, hydrogen mainly came from deionized water. At the same time, with the decrease of acetonitrile, the yield of the CO firstly increased, then decreased, and finally kept stable, which indicating that acetonitrile will not decompose in the system. When acetonitrile decreased from 27 mL to 24 mL, the reasons for the decrease of the yield of the CO may be due to the decrease in the volume of acetonitrile, which led to a decrease in the system of CO_2. When the acetonitrile and deionized water were 27 mL and 3 mL, the selectivity and yield of CO had reached the maximum, with 17.4 $\mu mol \cdot g^{-1}$ and 40 %, respectively. From an efficiently photocatalytic CO_2 reduction perspective, we hope to improve the selectivity of carbon products, so when acetonitrile and deionized water ratio is 27: 3, the optical catalytic performance of the system is better.

Table 1
Specific surface areas (S_{BET}), pore volumes, and pore diameter of three samples.

Samples	$S_{BET}(m^2/g)$	Pore Volume(cm^3/g)	Pore Diameter(nm)
TCN	25.8906	0.124480	25.7458
1.5 % CTN	31.9870	0.137798	22.3123

To evaluate the photocatalytic stability of CTN, we set up an experiment that changes over time (Fig. 4(e–f)). The experiments used 1.5 % CTN samples, added 24 mL acetonitrile and 6 mL deionized water, and illuminated 21 h under the light of 50 W. Within the initial 10 h, there are many catalyst surface activity sites, resulting in CO and CH_4 continuously increased. By 10 h, the yield of CO, CH_4 and H_2 was 71.9, 12.8 and 17.2 $\mu mol \cdot g^{-1}$, respectively. In the following 11 h, with the continuous increase of the time, the system tended to balance. At this time, the electron hole pairs had the best activity. The stability experiment fully showed that 1.5 % CTN had good catalytic stability. (Fig. S2) XRD test of catalyst before and after illumination shows that the position of diffraction peak does not change.

Finally, in order to verify whether the CTN catalyst worked in the CO_2 process, we set up 4 groups of control experiments (Fig. 5(a)). There were no CH_4, CO, and H_2 evolution without light irradiation and no catalyst, which indicated that there was a necessary condition of light irradiation and catalysts as a system of photocatalytic reduction. Without CO_2 in the system, there was only H_2 evolution, indicating that the water had also participated in the reduction process. In the absence of water and acetonitrile, the overall performance of photocatalysis decreased. It can also be seen that the presence of acetonitrile can increase the solubility of CO_2 and improve the selectivity of carbon products (Fig. S3). Fig. 5(b) shows the comparison of product selectivity between catalyst 1.5 % CTN and catalyst 2 % CTN. It can be found that catalyst 2 % CTN has a higher selectivity for CH_4, reaching 68 %, indicating that the increase of Cu content contributes to the formation of CH_4.

In Table 2, CTN remained better photocatalytic CO_2 reduction activity compared to previous works.

3.3. Photocatalytic mechanism

In order to evaluate the separation and transfer of photogenerated carriers, steady-state fluorescence tests and electrochemical tests were performed on the prepared materials. Fig. 6(a) shows that the lower PL intensity of CTN indicated that metal copper has greatly decreased carrier recombination rate. Among all CTN samples, 1.5 % CTN samples

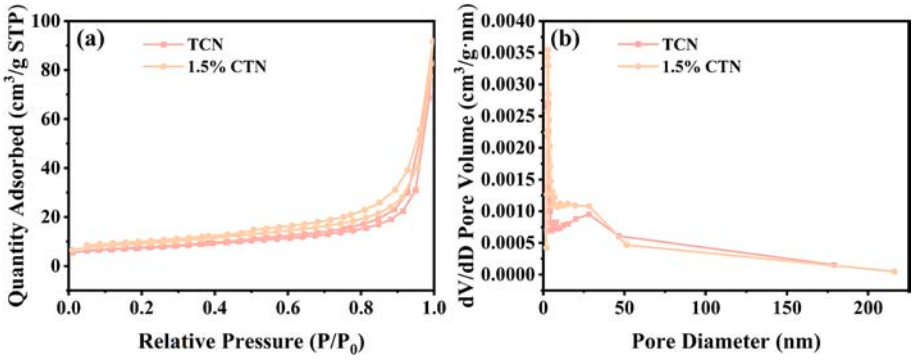

Fig. 3. (a) BET adsorption–desorption isotherms and (b) the pore dimension distribution curves of samples.

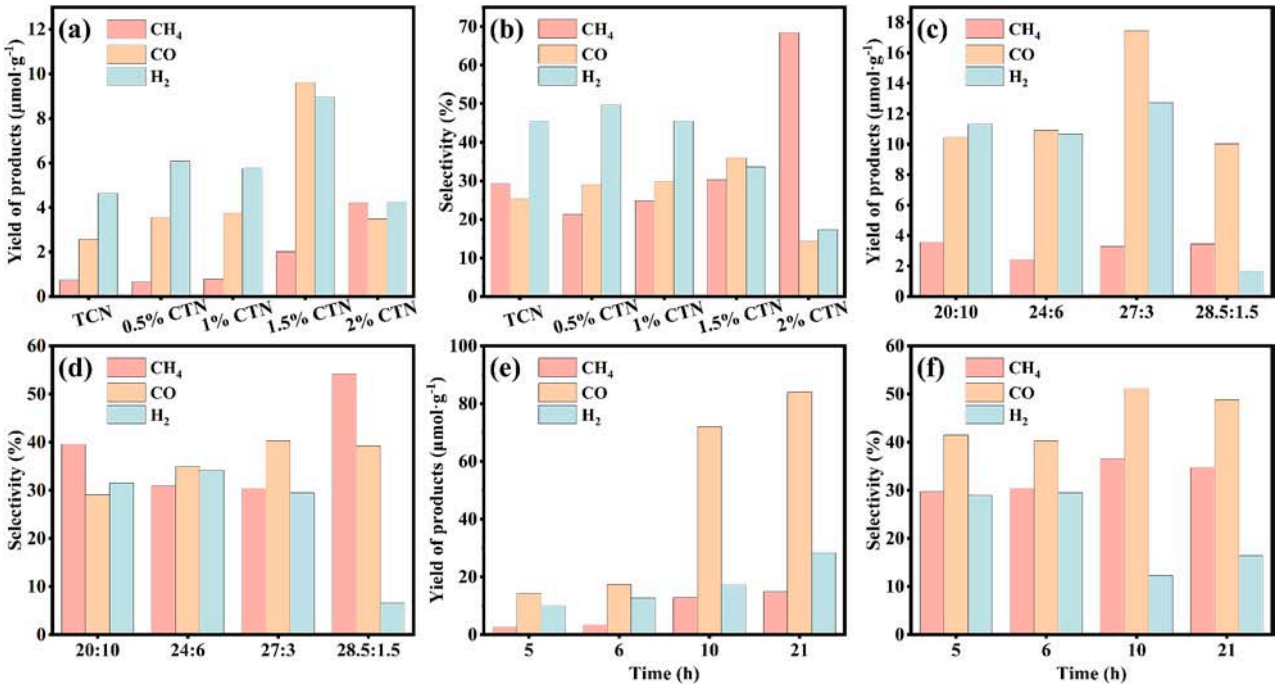

Fig. 4. CO_2 reduction experiments for all samples: (a) yield; (b) selectivity; CO_2 reduction experiments with different acetonitrile and deionised water ratio: (c) yield; (d) selectivity; stability experiment of 1.5% CTN: (e) yield; (f) selectivity.

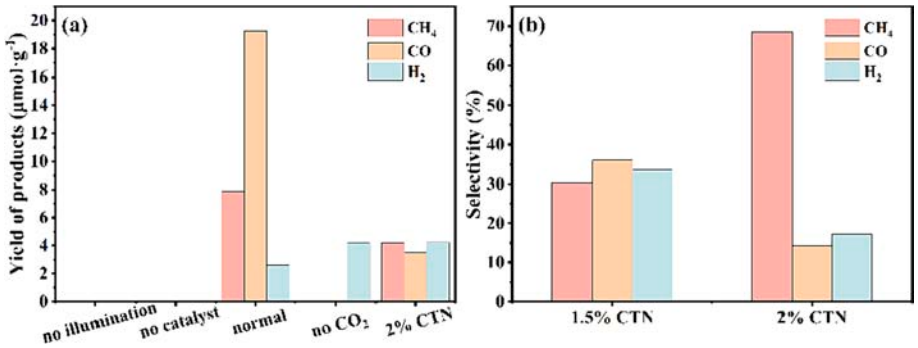

Fig. 5. (a)Control study of CO_2 reduction under different condition; (b) Comparison of selectivity of photocatalyzed CO_2 reduction products of samples 1.5 %CTN and 2 %CTN.

Table 2
Comparison of CO_2 reduction activity of g-C_3N_4-based catalysts.

Catalyst	Reaction conditions	Light	Photocatalytic activity	references
CeO_2/g-C_3N_4	CO_2; H_2O	300 W Xe	CO 0.590 μmol·h^{-1} CH_4 0.694 μmol·h^{-1}	[28]
g-C_3N_4-TiO_2	1.50 g $NaHCO_3$; 5.0 mL 4 M H_2SO_4	300 W Xe	CO 0.84 μmol g^{-1}·h^{-1} CH_4 5.21 μmol g^{-1}·h^{-1}	[29]
Pt–g-C_3N_4 /$KNbO_3$	CO_2; 2 mL H_2O	300 W Xe	CH_4 0.25 μmol·h^{-1}	[30]
Amine-functionalized g-C_3N_4	0.084 g $NaHCO_3$; 0.3 mL 2 M H_2SO_4	300 W Xe	CH_4 0.34 μmol g^{-1}·h^{-1} CH_3OH 0.28 μmol g^{-1}·h^{-1}	[31]
Mg-doped g-C_3N_4	CO_2; H_2O	300 W Xe	CO 12.97 μmol·g^{-1} CH_4 7.62 μmol·g^{-1}	[32]
Cu modified S-doped g-C_3N_4	CO_2; H_2O	500 W Xe	CO 9.6 μmol·g^{-1} CH_4 2.33 μmol·g^{-1}	[33]
Cu/g-C_3N_4	CO_2; H_2O; C_2H_3N	50 W LED	CO 11.55 μmol·g^{-1} CH_4 4.72 μmol·g^{-1}	This work

have the lowest PL intensity, indicating that its electron-hole pair separation rate is the highest. In general, it is useful to improve the optical catalytic performance through load copper. The EIS (Fig. 6(b)) shows that 1.5 % CTN has the smallest, demonstrating the least resistance during charge transfer. 1.5 % CTN also shown the highest transient photocurrent response (Fig. 6(c)). Meanwhile, 1.5 % CTN showed higher current density in the linear sweep voltammetry (Fig. 6(d)). The introduction of Cu can expansion the capture of light and promote the separation and transfer of photoinduced e^--h^+ pairs.

The optical properties of the catalysts were studied by UV–vis light absorption spectra (Fig. 7(a)). Compared with TCN, the CTN shown enhanced light absorption at the wavelengths greater than 450 nm. In addition, the absorption edge of CTN had red shift in comparison to TCN. The results of the UV–vis experiment can calculate the width of different catalysts. (Fig. S4) And the photocatalytic performance of the catalyst under different wavelengths of light is corresponding to it. The band gap was determined by the Tauc plots were calculated by equation: $(\hat{I} \pm h\hat{I}½)^n = A(h\hat{I}½\text{-}Eg)$ [34]. The curve is shown in Fig. 7(b). The calculated band gap values of TCN, 0.5 % CTN, 1 % CTN, 1.5 % CTN, and 2 % CTN are 2.59 eV, 2.47 eV, 2.44 eV, 2.33 eV and 2.42 eV,

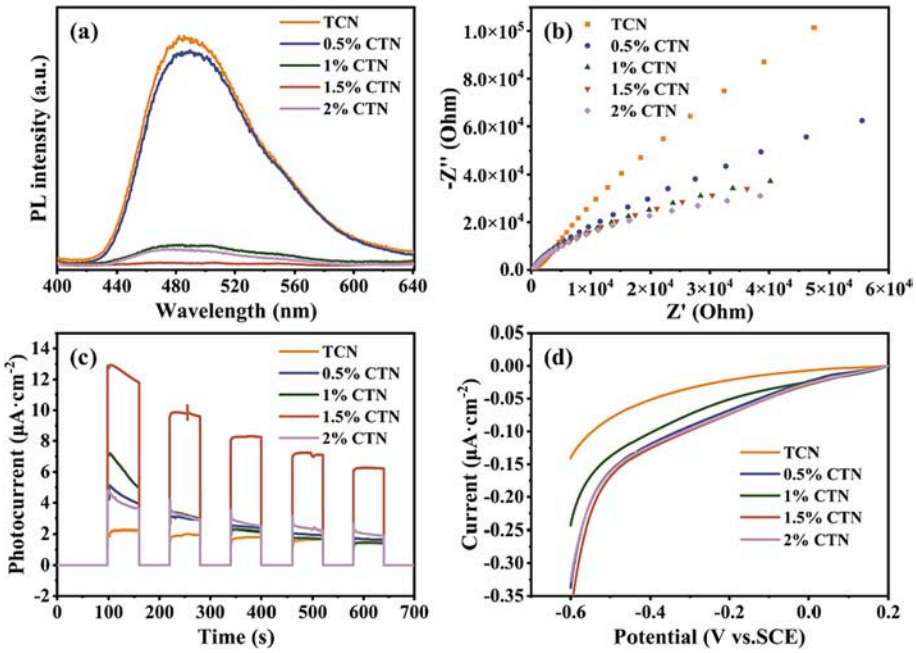

Fig. 6. (a) PL spectra; (b) EIS Nyquist plots; (c) transient photocurrent density response and (d) linear sweep voltammetry of all the samples prepared.

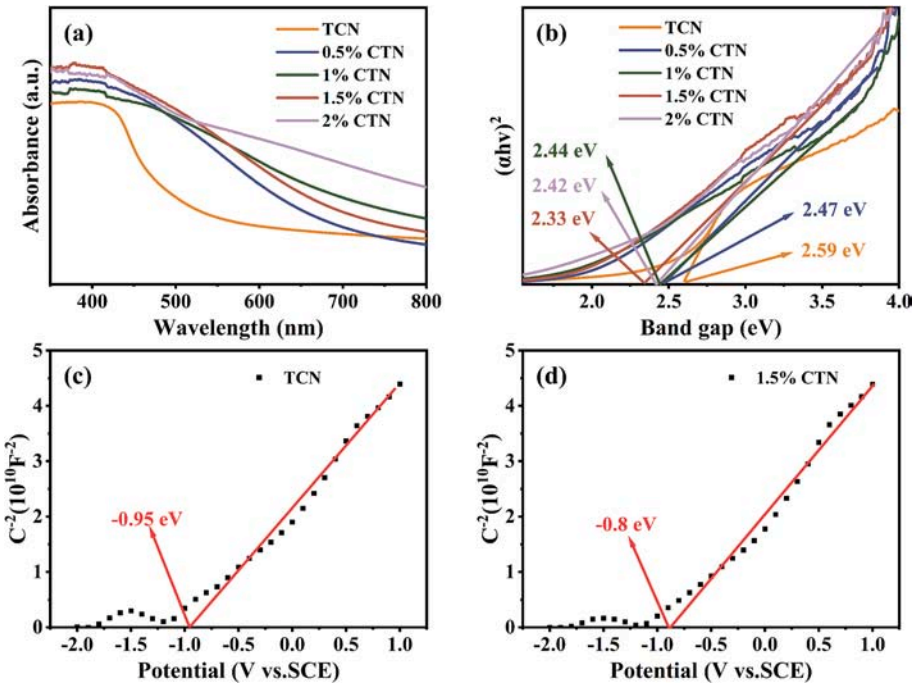

Fig. 7. (a) UV–vis light absorption spectra and (b) the corresponding Tauc plot of TCN, 0.5% CTN, 1% CTN, 1.5% CTN and 2% CTN; (c) Mott–Schottky plots of TCN; (d) Mott–Schottky plots of 1.5% CTN.

respectively. The formation of the pipe structure enhances the multiple reflexes of incident light in the material, increasing the light absorption range of the catalyst, and reducing the width of the band. At the same time, compared with TCN, introduction of Cu particles contributes to the generation of impurities energy levels, which has promoted the light capture of composite materials to a certain extent. These results show that the CTN sample has enhanced visible light absorption capabilities, resulting in more electronic empty acupoint loads. It can be predicted that because more photochemical electrons participating in CO_2 reduction, CTN samples may have a better optical catalytic performance than the original TCN. In Fig. 7(c–d), the MS plots of TCN and 1.5 % CTN have been measured. The results show that compared to the Ag/AgCl electrode, the CB potentials of TCN and 1.5 % CTN are −0.95 and −0.8 eV, respectively. In fact, the flat band (E_{fb}) potential is located near CB for n-type semiconductor with positive slope in the MS curve [35]. Therefore, the TCN and 1.5 % CTN belong to n-type semiconductor according to the slope of MS curve. After conversion, compared with normal hydrogen electrode (NHE), the CB potentials of TCN and 1.5 % CTN is −0.75 and −0.6 eV, respectively [36]. According to the band gaps of TCN and 1.5 % CTN, VB locations of TCN and 1.5 % CTN are 1.84 and 1.73 eV, respectively.

Fig. 8 shows that the feasibility mechanism of photocatalytic CO_2

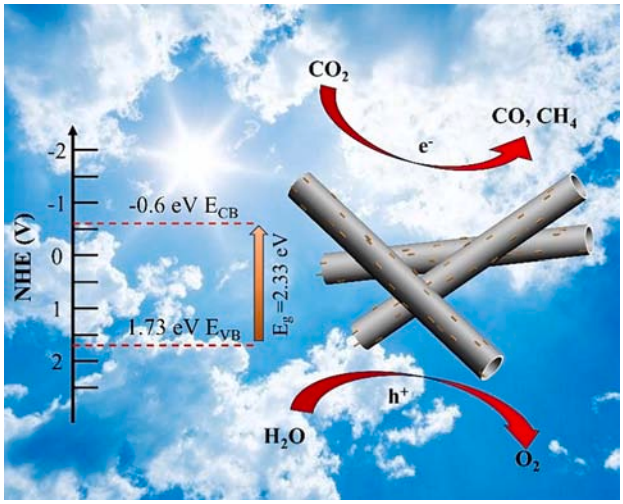

Fig. 8. Possible photocatalytic mechanism over CTN.

reduction of CTN. When the material is exposed to light, the photo-generated e^- are excited to the CB. At the same time, h^+ are left in the VB of CTN, which would oxidize H_2O to H^+. Cu is the capture sites and catalytic site of CO_2, and the photogenerated e^- are further transfer to Cu surface to induce the CO_2 reduction to CO and CH_4. The main CO_2 reduction steps are summarized as follows:

$$CO_2 + 2H^+ + 2e^- \rightarrow CO + H_2O$$

$$CO_2 + 8H^+ + 8e^- \rightarrow CH_4 + 2H_2O$$

In conclusion, the introduction of Cu enlarges the light absorption range and prolongs the carrier lifetime, which synergistically improves the photocatalytic activity [37].

4. Conclusions

In summary, we prepared the CN precursor used melamine as the sources through hydrothermal synthesis, and further form a Cu-doped g-C_3N_4 tubular sample mixes. The photocatalytic CO_2 reduction activity and selectivity of CTN photocatalysts have been significantly improved compared to that of TCN. The results showed that the CH_4 yields of 2 % CTN samples were high and have 68 % selectivity, which were higher than TCN samples without Cu doped. Mechanism analysis show that Cu can provide the active site and serve as an electron capture trap to effectively adjust the electronic structure of the g-C_3N_4, that would be contributed to CH_4 evolution. The work proposes a Cu modified C_3N_4 tubular material, which shows a method for designing C_3N_4-based high efficiency photocatalysts.

CRediT authorship contribution statement

Ye Liu and Lei Zhang conceived and designed the experiments. Ye Liu, Lei Zhang, Yubo Kuang, Xiaoqian Xiang, Guangran Di and Xiaojing Yin performed the experiments. Haohan Tao gave guidance on the writing and grammar of the paper. Xiaojun Lv and Meicheng Li contributed reagents/materials and analysis tools.

Declaration of competing interest

The authors declare that they have no known competing financial interests or personal relationships that could have appeared to influence the work reported in this paper.

Data availability

No data was used for the research described in the article.

Acknowledgements

The authors are grateful for the financial support by the National Key R&D Program of China under grant number 2020YFA0710404, and the innovative talents of NCEPU.

References

[1] K.R. Reddy, C.H.V. Reddy, M.N. Nadagouda, et al., Polymeric graphitic carbon nitride (g-C3N4) based semiconducting nanostructured materials: synthesis methods, properties and photocatalytic applications, J. Environ. Manage. 238 (2019) 25–40, https://doi.org/10.1016/j.jenvman.2019.02.075.
[2] A. Fujishima, K. Honda, Electrochemical photolysis of water at a semiconductor electrode, Nature 238 (1972) 37–38, https://doi.org/10.1038/238037a0.
[3] F. Li, L. Zhang, J. Tong, et al., Photocatalytic CO_2 conversion to methanol by Cu_2O/graphene/TNA heterostructure catalyst in a visible-light-driven dual-chamber reactor, Nano Energy 27 (2016) 320–329, https://doi.org/10.1016/j.nanoen.2016.06.056.
[4] K. Lizuka, T. Wato, Y. Miseki, et al., Photocatalytic reduction of carbon dioxide over Ag cocatalyst-loaded ALa4Ti4O15(A = Ca, Sr and Ba) using water as a reducing reagent, J. Am. Chem. Soc. 133 (2011) 20863–20868, https://doi.org/10.1021/ja207586e.
[5] A.M. Mohammed, S.S. Mohtarc, F. Aziz, et al., Review of various strategies to boost the photocatalytic activity of the cuprous oxide-based photocatalyst, J. Environ. Chem. Eng. 9 (2021) 105–138, https://doi.org/10.1016/j.jece.2021.105138.
[6] J. Gao, Y. Zhou, Z. Li, et al., High-yield synthesis of millimetre-long, semiconducting carbon nitride nanotubes with intense photoluminescence emission and reproducible photoconductivity, Nanoscale 4 (2012) 3687–3692, https://doi.org/10.1039/C2NR30777D.
[7] J. Bao, W. Bai, M. Wu, et al., Template-mediated copper doped porous g-C_3N_4 for efficient photodegradation of antibiotic contaminants, Chemosphere 293 (2022) 133607, https://doi.org/10.1016/j.chemosphere.2022.133607.
[8] F. Hou, J. Liu, Y. Zhang, et al., Synthesis of metallic copper modified g-C_3N_4 by molecular self-assembly structure and its combined catalytic performance with activated sludge, Journal of Hazardous Materials 388 (2020) 121754, https://doi.org/10.1016/j.jhazmat.2019.121754.
[9] B. Tahir, M. Tahir, A.S. Amin, et al., Photo-induced CO_2 reduction by CH_4/H_2O to fuels over Cu-modified g-C_3N_4 nanorods under simulated solar energy, Appl. Surf. Sci. 419 (2017) 875–885, https://doi.org/10.1016/j.apsusc.2017.05.117.
[10] G. Shi, L. Yang, Z. Liu, et al., Photocatalytic reduction of CO_2 to CO over copper decorated g-C_3N_4 nanosheets with enhanced yield and selectivity, Appl. Surf. Sci. 427 (2018) 1165–1173, https://doi.org/10.1016/j.apsusc.2017.08.148.
[11] T. Zhang, J. Low, X. Huang, et al., Copper-decorated microsized nanoporous titanium dioxide photocatalysts for carbon dioxide reduction by water, ChemCatChem 9 (2017) 3054–3062, https://doi.org/10.1002/cctc.201700512.
[12] W. Yu, D. Xu, T. Peng, Enhanced photocatalytic activity of g-C_3N_4 for selective CO_2 reduction to CH_3OH via facile coupling of ZnO: a direct Z-scheme mechanism, J. Mater. Chem. A 3 (2015) 19936–19947, https://doi.org/10.1039/C5TA05503B.
[13] S. Zhou, Y. Liu, J. Li, et al., Facile in situ synthesis of graphitic carbon nitride (g-C3N4)-N-TiO2 heterojunction as an efficient photocatalyst for the selective photoreduction of CO2 to CO, Appl Catal B 158–159 (2014) 20–29, https://doi.org/10.1016/j.apcatb.2014.03.037.
[14] K.-L. Bae, J. Kim, C.K. Lim, et al., Colloidal zinc oxide-copper(I) oxide nanocatalysts for selective aqueous photocatalytic carbon dioxide conversion into methane, Nat. Commun. 8 (2017) 11–56, https://doi.org/10.1038/s41467-017-01165-4.
[15] J.A. Torres, J.C. da Cruz, A.E. Nogueira, et al., Role of Cu^0-TiO_2 interaction in catalyst stability in CO_2 photoreduction process, J. Environ. Chem. Eng. 10 (2022) 107291, https://doi.org/10.1016/j.jece.2022.107291.
[16] T. Muhammad, C. Chuanbao, F.K. Butt, et al., Tubular graphitic-C_3N_4: a prospective material for energy storage and green photocatalysis, J. Mater. Chem. A 1 (2013) 13949–13955, https://doi.org/10.1039/C3TA13291A.
[17] Y. Huang, L. Yang, W. Huang, et al., Mesoporous tubular g-C_3N_4 as an efficient metal-free photocatalyst with peroxymonosulfate to degrade carbamazepine, Journal of Hazardous Materials Letters 4 (2023) 100081, https://doi.org/10.1016/j.hazl.2023.100081.
[18] W. Xie, K. Li, X.-H. Liu, et al., P-mediated Cu–N_4 sites in Carbon nitride realizing CO_2 photoreduction to C_2H_4 with selectivity modulation, Adv. Mater. 35 (2023) 2208132, https://doi.org/10.1002/adma.202208132.
[19] W.-J. Ong, L.-L. Tan, Y.H. Ng, et al., Graphitic carbon nitride (g-C3N4)-based photocatalysts for artificial photosynthesis and environmental remediation: are we a step closer to achieving sustainability? Chem Reviews 116 (2016) 7159–7329, https://doi.org/10.1021/acs.chemrev.6b00075.
[20] J. Zhang, Y. Chen, X. Wang, Two-dimensional covalent carbon nitride nanosheets: synthesis, functionalization, and applications, Energ. Environ. Sci. 8 (2015) 3092–3108, https://doi.org/10.1039/C5EE01895A.

[21] Q. Liang, Z. Li, Z.-H. Huang, et al., Holey graphitic carbon nitride nanosheets with carbon vacancies for highly improved photocatalytic hydrogen production, Adv. Funct. Mater. 25 (2015) 6885–6892, https://doi.org/10.1002/adfm.201503221.
[22] P. Niu, L. Zhang, G. Liu, et al., Graphene-like carbon nitride nanosheets for improved photocatalytic activities, Adv. Funct. Mater. 22 (2012) 4763–4770, https://doi.org/10.1002/adfm.201200922.
[23] P. Niu, G. Liu, H.-M. Cheng, Nitrogen vacancy-promoted photocatalytic activity of graphitic carbon nitride, J. Phys. Chem. C 116 (2012) 11013–11018, https://doi.org/10.1021/jp301026y.
[24] L. Jing, R.X. Zhu, D.L. Phillips, et al., Effective prevention of Charge trapping in graphitic Carbon nitride with nanosized red phosphorus modification for Superior photo(electro)catalysis, Adv. Funct. Mater. 27 (2017) 1703484, https://doi.org/10.1002/adfm.201703484.
[25] W.J. Wang, G.Y. Li, T.C. An, et al., Photocatalytic hydrogen evolution and bacterial inactivation utilizing sonochemical-synthesized g-C_3N_4/Red phosphorus hybrid nanosheets as a wide-spectral-responsive photocatalyst: the role of type I band alignment, Appl Catal B 238 (2018) 126–135, https://doi.org/10.1016/j.apcatb.2018.07.004.
[26] D.J. Martin, K.P. Qiu, S.A. Shevlin, et al., Highly efficient photocatalytic $_H$2 evolution from water using visible light and structure-controlled graphitic Carbon nitride, Angew. Chem. Int. Ed. 53 (2014) 9240–9245, https://doi.org/10.1002/anie.201403375.
[27] P. Liu, E.J.M. Hensen, Highly efficient and robust Au/$MgCuCr_2O_4$ catalyst for GasPhase oxidation of ethanol to acetaldehyde, J. Am. Chem. Soc. 135 (2013) 14032–14035, https://doi.org/10.1021/ja406820f.
[28] S.E. Korkut, H. Kucukkececi, O. Metin, Mesoporous graphitic Carbon nitride/black Phosphorus/AgPd alloy Nanoparticles Ternary nanocomposite: a highly efficient catalyst for the methanolysis of ammonia borane, ACS Appl Mater Interfaces 12 (2020) 8130–8139, https://doi.org/10.1021/acsami.9b18917.
[29] D.A. Reddy, E.H. Kim, M. Gopannagari, et al., Few layered black phosphorus/MoS_2 nanohybrid: a promising co-catalyst for solar driven hydrogen evolution, Appl Catal B 241 (2019) 491–498, https://doi.org/10.1016/j.apcatb.2018.09.055.
[30] Z. Ai, M. Huang, D. Shi, et al., Phase engineering of CdS optimized by BP with p-n junction: establishing spatial-gradient charges transmission mode toward efficient photocatalytic water reduction, Appl Catal B 315 (2022) 121577, https://doi.org/10.1016/j.apcatb.2022.121577.
[31] M. Li, L. Zhang, M. Wu, et al., Mesostructured CeO_2/g-C_3N_4 nanocomposites: remarkably enhanced photocatalytic activity for CO_2 reduction by mutual component activations, Nano Energy 19 (2016) 145–155, https://doi.org/10.1016/J.NANOEN.2015.11.010.
[32] K. Li, B. Peng, J. Jin, et al., Carbon nitride nanodots decorated brookite TiO_2 quasi nanocubes for enhanced activity and selectivity of visible-light-driven CO_2 reduction, Appl Catal B 203 (2017) 910–916, https://doi.org/10.1016/j.apcatb.2016.11.001.
[33] H. Shi, C. Zhang, C. Zhou, et al., Conversion of CO_2 into renewable fuel over Pt-g-C_3N_4/$KNbO_3$ composite photocatalyst, RSC Adv. 5 (2015) 93615–93622, https://doi.org/10.1039/C5RA16870H.
[34] Q. Huang, J. Yu, S. Cao, et al., Efficient photocatalytic reduction of CO_2 by amine-functionalized g-C_3N_4, Appl. Surf. Sci. 358 (2015) 350–355, https://doi.org/10.1016/j.apsusc.2015.07.082.
[35] X. Dong, S. Zhang, H. Wu, et al., Facile one-pot synthesis of mg-doped g-C_3N_4 for photocatalytic reduction of CO_2, RSC Adv. 9 (2019) 28894–28901, https://doi.org/10.1039/C9RA04606B.
[36] N. Ojha, A. Bajpai, S. Kumar, Visible light-driven enhanced CO_2 reduction by water over Cu modified S-doped g-C_3N_4, Cat. Sci. Technol. 9 (2019) 4598–4613, https://doi.org/10.1039/C9CY01185D.
[37] C. Lv, Z. Yin, X. Yang, et al., A [001]-oriented hittorf`s phosphorus nanorods/polymeric carbon nitride heterostructure for boosting wide-spectrum-responsive photocatalytic hydrogen evolution from pure water, Angew. Chem. Int. Ed. 59 (2020) 868–873, https://doi.org/10.1002/anie.201911503.